/afm

PS/AA/Note 85-14
11.11.1985

CALCULATIONS OF BEAM ENERGY DEPOSITION, ADIABATIC TEMPERATURE RISE AND THERMAL STRESS IN THE WINDOWS OF HIGH DENSITY PASSIVE TARGETS

by

T. W. Eaton, F. Gamba, M. Möller, G.R. Stevenson

In order to assess the performance of windows for the new high density target, illustrated by Fig. 1, FLUKA 82 computations have been made of the energy deposition in the two windows of the high density target, for a range of materials including aluminium alloy 6061, titanium alloy UTA 6V, Nimonic 105 and Acier 37. The downstream window thickness was taken, in all cases, to be 4 mm, and the upstream 2 mm. A gaussian beam distribution was assumed with σ = 1.118 mm, impinging on a 5 cm long tungsten target of diameter 3 mm, with a 6 mm carbon plug between the tungsten and the downstream window.

The results obtained for the downstream windows are summarized in Fig. 2, where energy deposition in GeV per cm^3 is plotted as a function of radial distance from the centre of the window. The energy deposition for Acier 37 and Nimonic 105 are very similar, and would require very long and expensive computer runs to separate. The present runs were already of 100 minute duration, each costing 350 SF.

A comparison between the high accuracy FLUKA 82 runs and those obtained using the "rule of thumb" value for energy deposition, of 2 MeV gm^{-1} cm^2, is shown in Fig. 2b). The FLUKA 82 upstream values are seen to be approximately twice the values obtained by the rule of thumb method and this is due to the latter method only considering ionization and excitation processes, which are seen to make up only 50% of the total energy loss, other mechanisms being electromagnetic cascade generation and nuclear rather than atomic excitation. The downstream values start off, at low Z, approximately equal to the rule of thumb values, but increase markedly with Z, due to the increasing energy absorption from the lower energy cascade products which is highly Z dependent.

In order to utilize the results of Fig. 2, information already available from DOT computations by Poncet, was noted. These are summarized in Fig. 3, where the steady state temperature distribution in the target model type E (Fig. 1) is shown schematically. It will be seen that the steady state centre window temperature is 540°C, therefore all relevant material parameters must be known as a function of temperature. These are summarized for the materials in question in Figs 4-6 up to a maximum steady state temperature of 800°C.

The energy depositions were translated into temperature distributions, immediately after the beam pulse, using the general purpose heat transfer DOT programme. The temperature dependence of the thermal conductivity and the specific heat capacity given in Figs 4-6 were utilized to give the corresponding maximum temperature distributions shown in Figs 7-9. The associated radial and azimuthal stresses (σ_r and σ_θ) were then evaluated using the SAP V programme, which essentially evaluates static or dynamic stresses in linear structural systems. In this evaluation, the temperature dependence of the modulus of elasticity and the coefficient of thermal expansion were utilized and it was assumed that the outer boundary of the window was mechanically restrained.- The equivalent stress σ_e may then be evaluated bearing in mind that, in this particular problem, all shear stresses have been assumed to be equal to zero. The SAP V results are plotted in Figs 10-12 for σ_r and σ_θ separately. The equivalent stress σ_e, following the Von Mises strength theory, is given by the equation:

$$\sigma_e = (\sigma_r^2 + \sigma_\theta^2 - \sigma_r\sigma_\theta)^{1/2}$$

One final procedure, however, was necessary before the thermally induced stresses could be compared with the temperature dependent yield stress in each case. This procedure was for making allowance for the fact that the DOT programme assumed a steady state temperature of 20°C whereas it is known that the window of the target is actually at 550°C. Allowance was made crudely by multiplying all of the resultant stresses by a factor X being the ratio of the relevant parameters of the material at the temperature T compared to their values at 20°C. Evidently, X = 1.000 at 20°C and decreased to approximately 0.6 at 800°C for the particular case of Nimonic 105.

Figure 13 shows the ratio of thermal stress against yield stress plotted as a function of steady state window temperature for Acier 37, titanium alloy and for Nimonic 105. Several crucial conclusions can be reached from these curves:

A) The ratio of σ_e to $\sigma_{0,2}$ is relatively high, even at room temperature, but could be tolerated from a fatigue point of view if the particular material has good fatigue characteristics, as have the titanium alloy and Nimonic 105.

B) A downstream window of Acier 37 would fail relatively quickly at these stress levels, especially since the steady state temperature of the window is known to be 550°C. At this temperature the stress ratio for this material is 0.63 and it is well known that Ac 37 has poor fatigue characteristics at elevated temperatures and at these cyclic stress levels.

C) The behaviour of UTA 6V titanium alloy will be acceptable up to 400°C and then progressively get worse. It therefore appears that the titanium windows are on the limit under the conditions imposed on them at the moment i.e. T_{SS} = 550°C, I = 10^{13} p.p.p., $\sigma_{THERMAL}$ = 0.5 $\sigma_{0,2}$. Any increase in T_{SS} or I would cause the window to fail. In support of this point, the literature shows that a cyclic stress of 510 Nmm^{-2}, i.e. 0.6 $\sigma_{0,2}$ at room temperature, gives a cyclic stress lifetime of 10^8 cycles, but any increase in temperature severely reduces the lifetime. An arrangement of target components which will allow the beam intensity to be increased without increasing T_{SS} or $\sigma_{THERMAL}$ is discussed in a later section.

D) Nimonic 105 has an interesting characteristic and strongly suggests that such a material might perhaps be useful, if the passive target were preheated to its working temperature before beam pulsing. For example, if the T_{SS} value were 800°C, as could be envisaged if the PS intensity were increased to say 1.6 × 10^{13} p.p.p., then the $\sigma_{THERMAL}$ = 0.82 $\sigma_{0,2}$, whereas it would be 1.16 $\sigma_{0,2}$ for titanium alloy, which is known to have somewhat poorer fatigue characteristics also.

E) The performance of aluminium alloy windows are interesting in that it is evidently out of the question to use them for high density passive targets and yet they have performed well on the conventional copper targets. The reasons for this are fairly evident since, in the latter case, the T_{SS} value was less than 150°C and the cascade deposition due to the

copper, in the downstream window, is much less than with the high density target. This was verified by a FLUKA 82 of the conventional geometry, the results of which are shown in Fig. 13b). The peak deposited energy is 65% of that in the heavy duty target which leads via DOT and SAP V to radial and azimuthal stresses of 95 and 100 Nmm^{-2}, respectively. The resultant of these, when allowance was made for the DOT analysis, is 64 Nmm^{-2} for a T_{SS} of 100°C which gives $\sigma = 0.24\ \sigma_{0,2}$. The full thermal stress-steady state temperature characteristic for this window is given in Fig. 13c) and shows that a steady-state temperature above 250°C would be catastrophic. Clearly therefore a 6 mm aluminium alloy window, in a conventional 12 cm copper target, has a low ratio of thermal to yield stress and will therefore last for 10^8 to 10^9 cycles. This is comforting since this is exactly what is found in practice, verifying therefore the validity of these calculations.

Table 1 shows the fatigue characteristics of Nimonic 105, but under conditions of uniaxial stressing. They are, however, illustrative in that at, for example a temperature of 800°C, such a material could undergo a stress of the form $\sigma \pm 0.5\sigma$ where $\sigma = 400\ Nmm^{-3}$ ($0.55\ \sigma_{0,2}$ at that temperature) and survive for 3×10^7 cycles, which is a factor 10 more than endured in a 3 months PS run.

An ideal target window material will, however, be one that follows the titanium curve but up to 800-900°C before rising, or more realistically a material following a nimonic-like characteristic but at lower values (the dotted curve A of Fig. 13). Further material searches are therefore required but this investigation has suggested that it should not be fruitless since both nimonic and UTA 6V has certain good characteristics.

It is possible to predict, with a fair degree of accuracy, the full parameter list of this ideal material, nicknamed "Kavorite" after H.G. Wells. These are shown in Table 2 as a function of temperature. Likely candidates possessing the properties of Kavorite are a) a cobalt-aluminium alloy 50% atomic percentage of each, having a melting point of 1645°C, b) a titanium-aluminium alloy with the same percentage ratio's, having a melting point of 1460°C, c) a carbon-titanium alloy of 40% carbon, melting point 3000°C and d) aluminium-60% nickel, melting point 1575°C, e) a zirconium-vanadium alloy with addition to prevent oxidation, and finally f) a niobium -10% tungsten alloy Cb-752.

Calculations of upstream window energy deposition have not been discussed because, in this case, the effect is due entirely to the primary beam, producing much less effect than with the downstream window. However, to illustrate this, the energy deposited in the 2 mm titanium window, out to 1.0 and 2.0 mm radial distance, were respectively 39% and 30% of the corresponding figures for the 4 mm downstream one. The corresponding values for the nimonic windows were 58% and 49.8%. Furthermore it is known that the upstream window is at a steady state temperature of only 30-40°C, at centre. The above considerations of target window materials lead to the following proposals regarding the target itself.

1. *THE TARGET MATERIAL SHOULD BE AXIALLY SEPARATED*

The purpose of this change is two fold: a) a separation of the target material, as for example shown in insert b) of Fig. 14, will allow more heat to flow out via the main target body rather than to the snout. This should therefore decrease the steady state temperature of the downstream window from 550°C to perhaps 350-400°C for 10^{13} p.p.p. b) FLUKA 82 computations of this geometry, summarized in Fig. 14, show that the adiabatic temperature rises at window centre drop to 60% of the value found in the conventional geometry. This is because of the greater spread of the cascade products, generated in the target material. The corresponding stresses will also therefore change accordingly to values at 400°C for titanium and nimonic of respectively 0.37 $\sigma_{0,2}$ and 1.04 $\sigma_{0,2}$, which is good for titanium since this is the minimum value but bad for nimonic, at least with 10^{13} p.p.p. However, upgrading the PS intensity to 2×10^{13} p.p.p. would reverse the situation, giving the situation for nimonic mentioned under D) of the last section, namely T_{SS} = 800°C, $I = 2 \times 10^{13}$ p.p.p. and $\sigma_{THERMAL} = 0.8\ \sigma_{0,2}$ (T). The energy deposition in the actual target material, for the two configurations, are shown in Figs. 15 and 16.

2. *THE TARGET MATERIAL SHOULD BE ENCLOSED IN A THIN WALL TANTALUM TUBE*

A rapid swelling of high density target material has been suggested recently[1]. It is proposed therefore that the whole of the target material should be enclosed in a 0.2-0.5 mm thin walled tantalum tube, such that little direct proton beam interaction occurs in the latter. This would then be able to resist the swelling which at the very least would lower the saturation value.

3. *THE TARGET EXTERNAL DESIGN SHOULD BE CHANGED, AS FOR EXAMPLE SHOWN IN FIGURE 17*

This design is presented for several reasons: 1) the spherical external and internal surfaces of the end window are much more efficient in withstanding the adiabatic stresses applied. 2) It is an exact fit to the inlet part to the 2 cm lithium lens so that intimate contact could be made with this device, such that cooling could then be by direct conduction through to a cold surface. Such a contact could be made via a water cooled interface piece placed between, but, in any case, should allow the target to be moved axially by approximately the extra amount required of 1.3 cm, partially at least making up for the loss in antiproton yield expected from procedure 1).

ACKNOWLEDGEMENTS

The authors wish to acknowledge the help given in this work by A. Poncet and H. Ravn, and also the kind permission given by P. Riboni in order to carry out the DOT and SAP V computations.

REFERENCE

1. T.W. Eaton, A Comparison between the Observed Decreases in Antiproton Yield from Passive Targets and the Theoretical Predictions Based Upon the Concept of Stress and Temperature Enhanced Void Growth., PS/AA/Note 85-9.

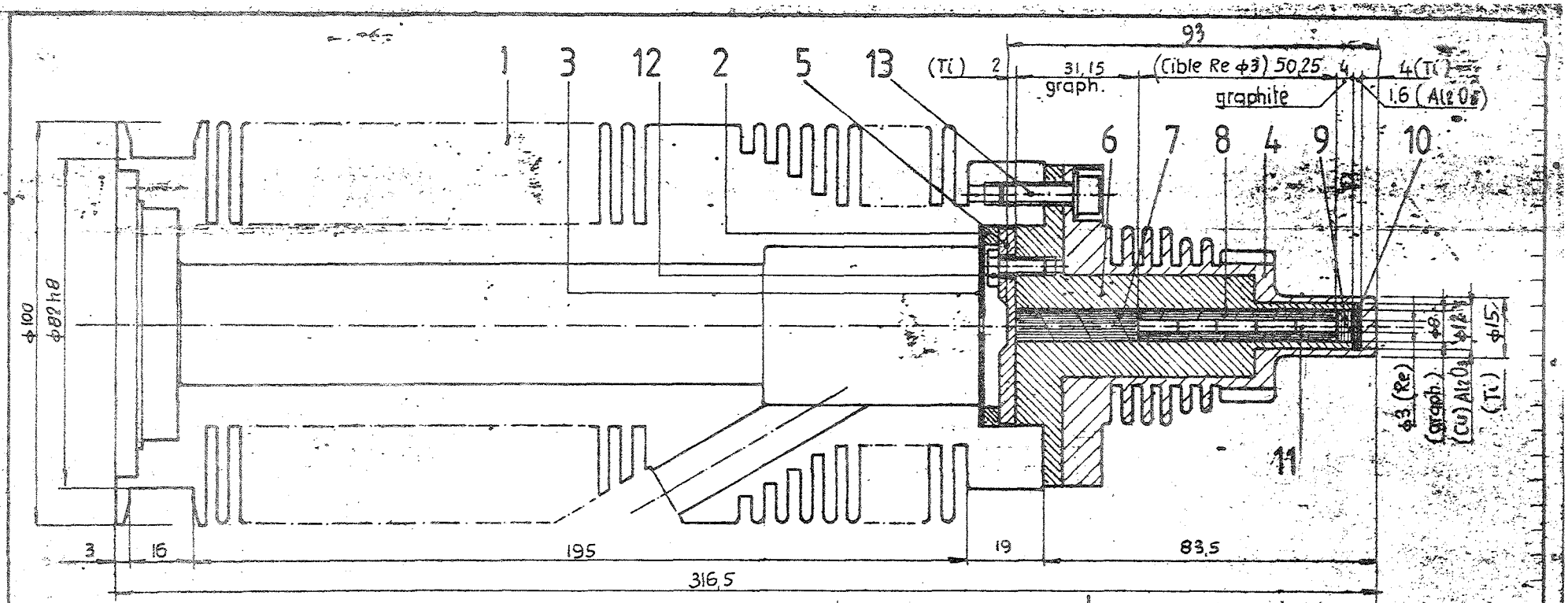

QUANT	DESCRIPTION	POS	MATIERE	OBSERVATIONS
	ENSEMBLE / ASSEMBLY		S. ENS./ S. ASSY.	
6	Vis tête cyl s.p.c. M6 x 20	13	Ac. inox A4	
6	Vis tête ex. M4 x 12	12	Ac. inox A4	
1	Cible ϕ3 x ~50 (5 x 10)	11	Re	5 pièces de long. ~10 à assembler
1	Disque ϕ12 g7 x ép. 2 $^{+0p5}_{0}$	10	Al_2O_3	A réaliser
1	Graphite droite	9		A60 · 3844 · 4 pos. 3
1	Graphite tube	8		A60 · 3844 · 4 pos. 2
1	Graphite gauche	7		A60 · 3844 · 4 pos. 4
1	Enveloppe	6		A60 · 3848 · 3 pos. 1
1	Fermeture	5		A60 · 3848 · 3 pos. 2
1	Extension	4		A60 · 3847 · 3
1	Ecran lumin. ϕ50 ϕ7 x ép. 1	3		A60 · 1005.4 pièce existante à modif.
1	Anneau	2		A60 · 3780 · 4
1	Corps	1		A60 · 3778 · 3

FIGURE 1 HIGH DENSITY PASSIVE TARGET, TYPE E, WITH COPPER SLEEVE AND TITANIUM ALLOY CASE.

Experience CIBLE PASSIVE - LENT. LITH.

ENS. CIBLE PASSIVE N°5

ECHELLE SCALE 1:1

	NOM	DATE
DESSINE	SETBA	SEPT. 1985
CONTROLE		oct 85
VU		
REMPLACE		

ORGANISATION EUROPEENNE POUR LA RECHERCHE NUCLEAIRE
EUROPEAN ORGANIZATION FOR NUCLEAR RESEARCH
GENEVE

PS

A60 - 3843 - 3 INDICE

INDICE	DATE	NOM	ZONE	MODIFICATION

FIGURE 2 a) ENERGY DEPOSITION IN 4 mm DOWNSTREAM TARGET WINDOWS

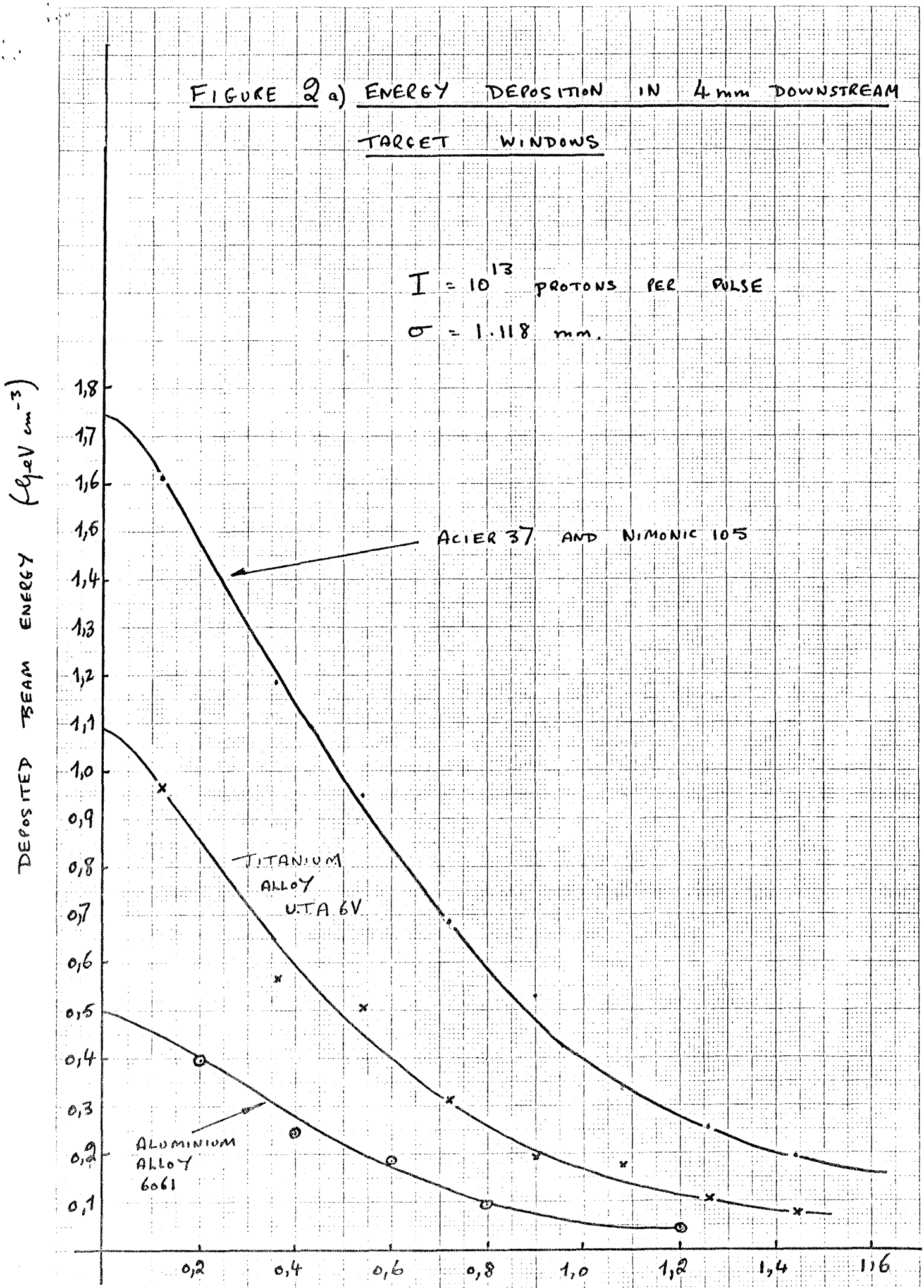

FIGURE 2 b) RATIO OF ENERGY DEPOSITION IN TARGET WINDOWS BY FLUKA 82, COMPARED TO VALUES ASSUMING A CONSTANT ENERGY DEPOSITION OF 2 MeV g^{-1} cm^2

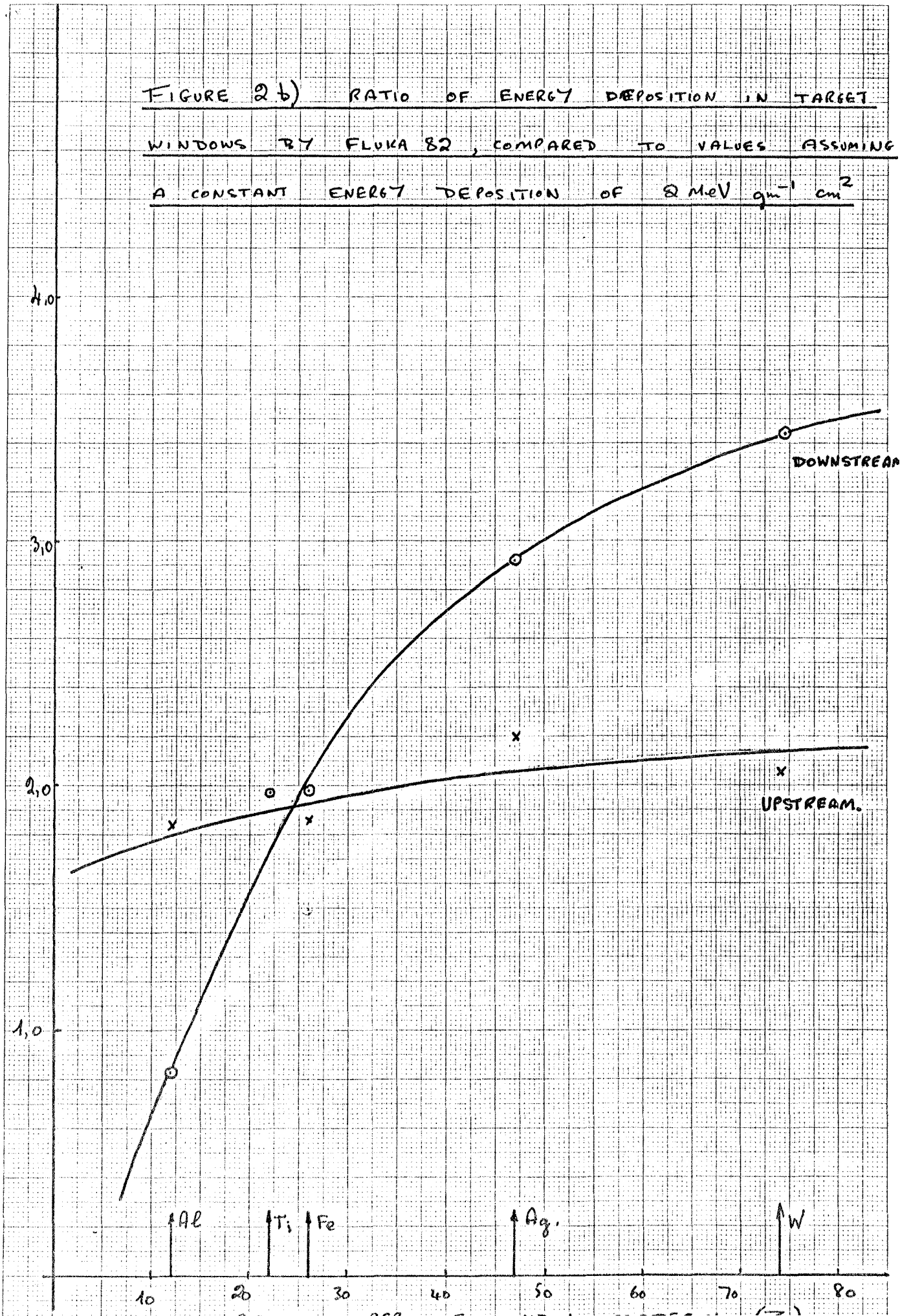

FIGURE 3. STEADY STATE TEMPERATURE DISTRIBUTION IN TYPE 6 HIGH DENSITY PASSIVE TARGET

$I = 10^{13}$ PROTONS PER PULSE.

(°C)

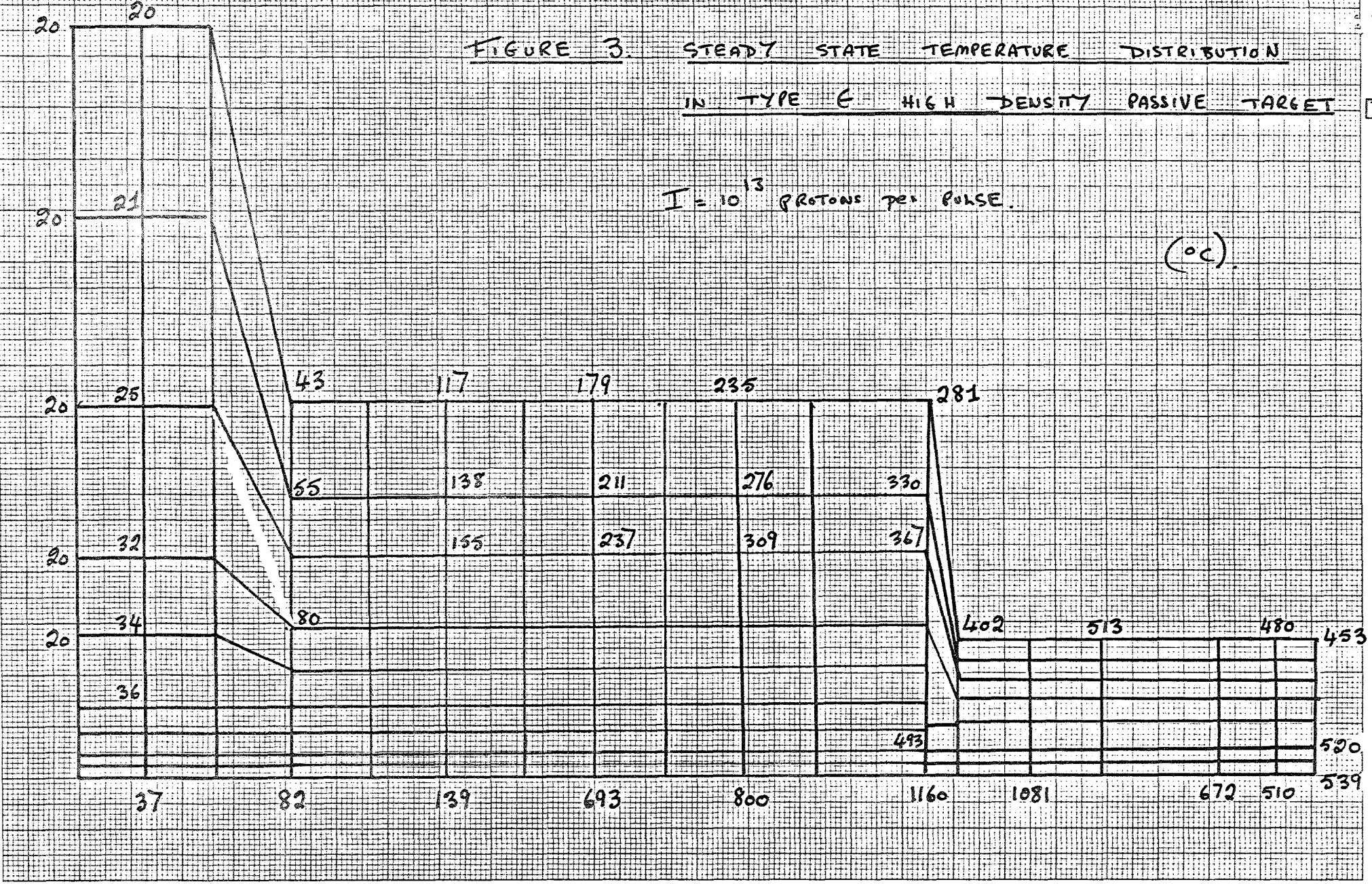

FIGURE 4. TEMPERATURE DEPENDANT PARAMETERS OF TARGET WINDOW.

WINDOW MATERIAL : TITANIUM ALLOY UTA 6V

RATURE °C.	20	100	200	300	400	500	600	700	800
TY cm^{-3}	4,43	4,42	4.41	4,39	4,38	4,37	4,36	4,34	4,33
FIC $^{-1}$ °C	0,546	0,575	0,601	0,636	0,689	0,737	0,802	0,878	0,953
AL TIVITY $^{-1}$ °C	6,7	7.1	9,63	11.3	12.6	13.4	13.6	13.8	14.1
R SION CIENT $^{-1}$ $\times 10^{-6}$	8.60	8.86	9.04	9.27	9.45	9.62	9.80	9.98	10.12
GS LUS mm^{-2}	110,000	106 000	100 500	95 000	88 500	82000	76 000	70 000	63000
D SS mm^{-2}	830	800	740	690	620	500	280	170	110

FIGURE 5. TEMPERATURE DEPENDANT PARAMETERS OF TARGET WINDOW.

WINDOW MATERIAL : ACIER 37

ATURE °C.	20	100	200	300	400	500	600	700	800
TY cm^{-3}	7.85	7.82	7.78	7.73	7.71	7.68	7.64	7.60	7.57
FIC $^{-1}$ °C	0.479	0.483	0,525	0,559	0.596	0.664	0,743	0.861	0.962
AL TIVITY $^{-1}$ °C	48	50	48.5	41.5					
R SION CIENT $\times 10^{-6}$	12.00	12.19	12.96	13.50	13.90	14.29	14.71	14.99	15.28
S LVS mm^{-2}	210,000	195,000	187000	183000	180000	160000	105000	60000	20,000
D SS mm^{-2}	290	265	238	196	165	131	76	37	10

FIGURE 6. TEMPERATURE DEPENDANT PARAMETERS OF TARGET WINDOW.

WINDOW MATERIAL: NIMONIC 105.

RATURE °C.	20	100	200	300	400	500	600	700	800
TY cm^{-3}	8.01	7.97	7.92	7.88	7.84	7.80	7.74	7.68	7.60
FIC $^{-1}$ °C	0.419	0.461	0.502	0,522	0.544	0.564	0.586	0.628	0,670
AL TIVITY $^{-1}$ °C	10.9	12.1	13.6	15.0	16.3	17.7	18.6	20.6	22.2
R SION CIENT $^{-1}$ $\times 10^{-6}$	12.2	12.5	12.8	13.1	13.4	13.7	14.0	15.3	18.0
GS LUS mm^{-2}	188,000	184,000	179,000	174 000	168,000	161 000	154000	139000	110 000
D SS mm^{-2}	826	811	785	772	783	785	775	778	718

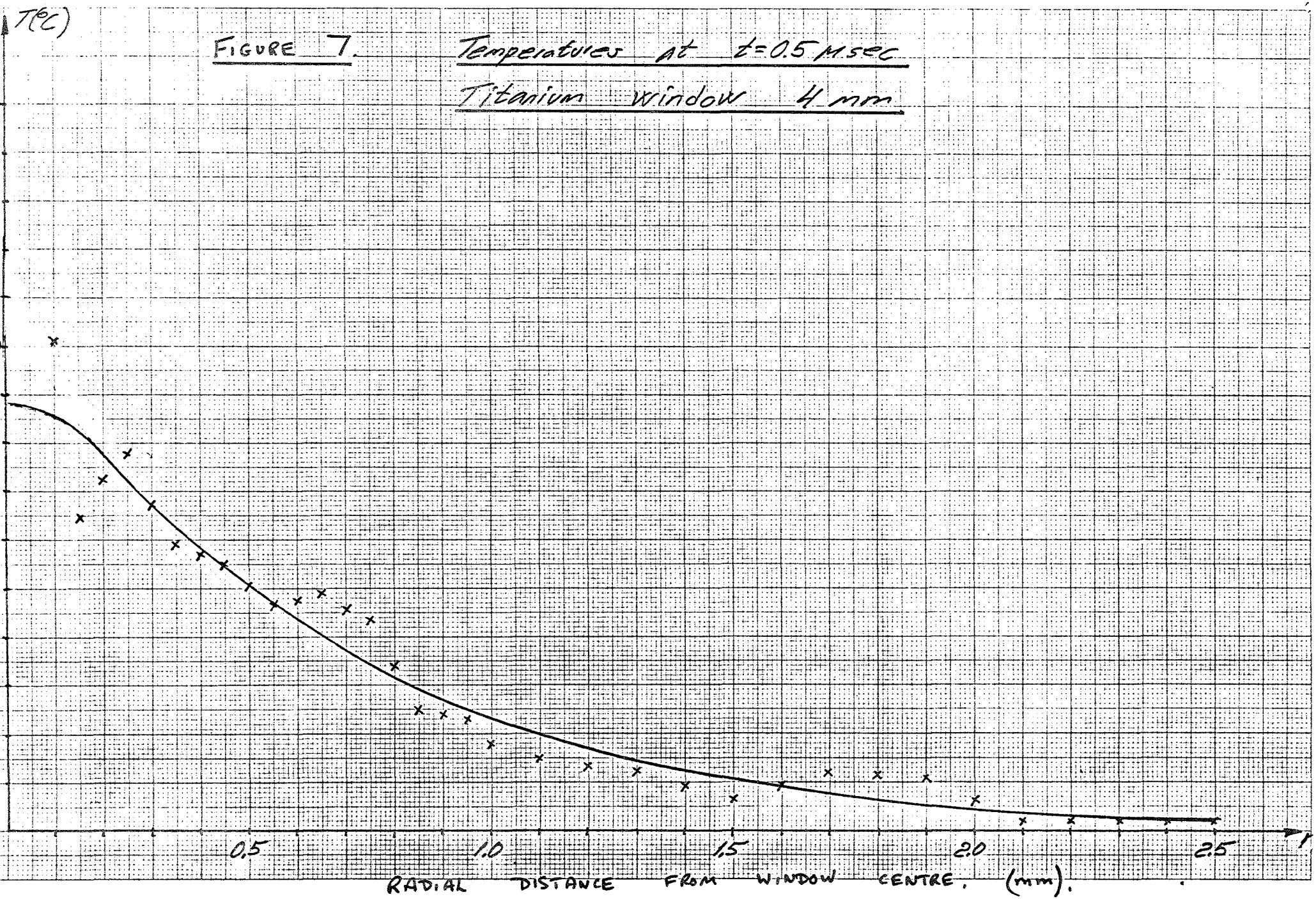

FIGURE 7. Temperatures at $t = 0.5$ msec

Titanium window 4 mm

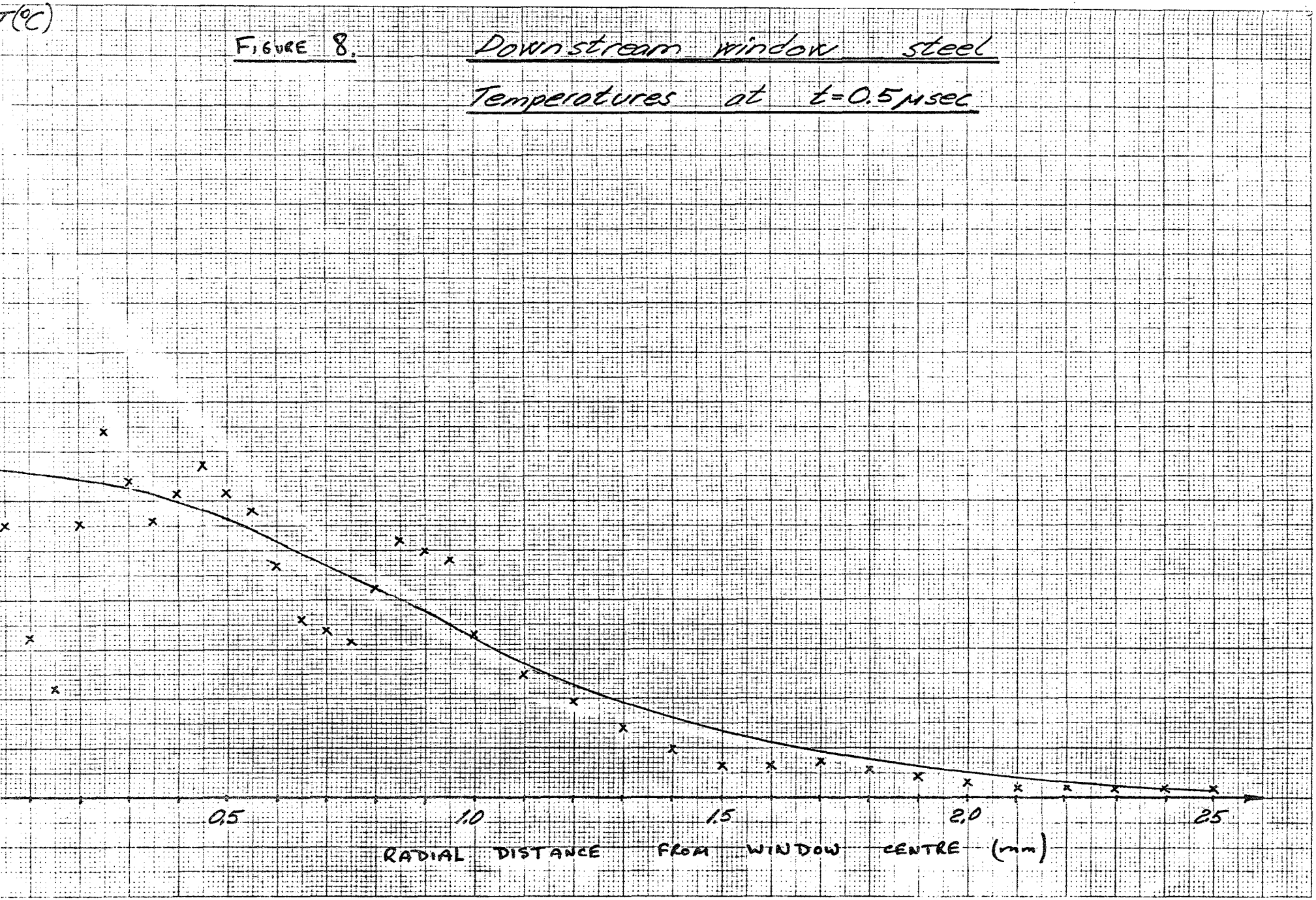

FIGURE 8. Downstream window steel Temperatures at t=0.5 msec

T(°C)

FIGURE 9. Temperatures at $t = 0.5\ \mu sec$

Nimonic Window, 4mm

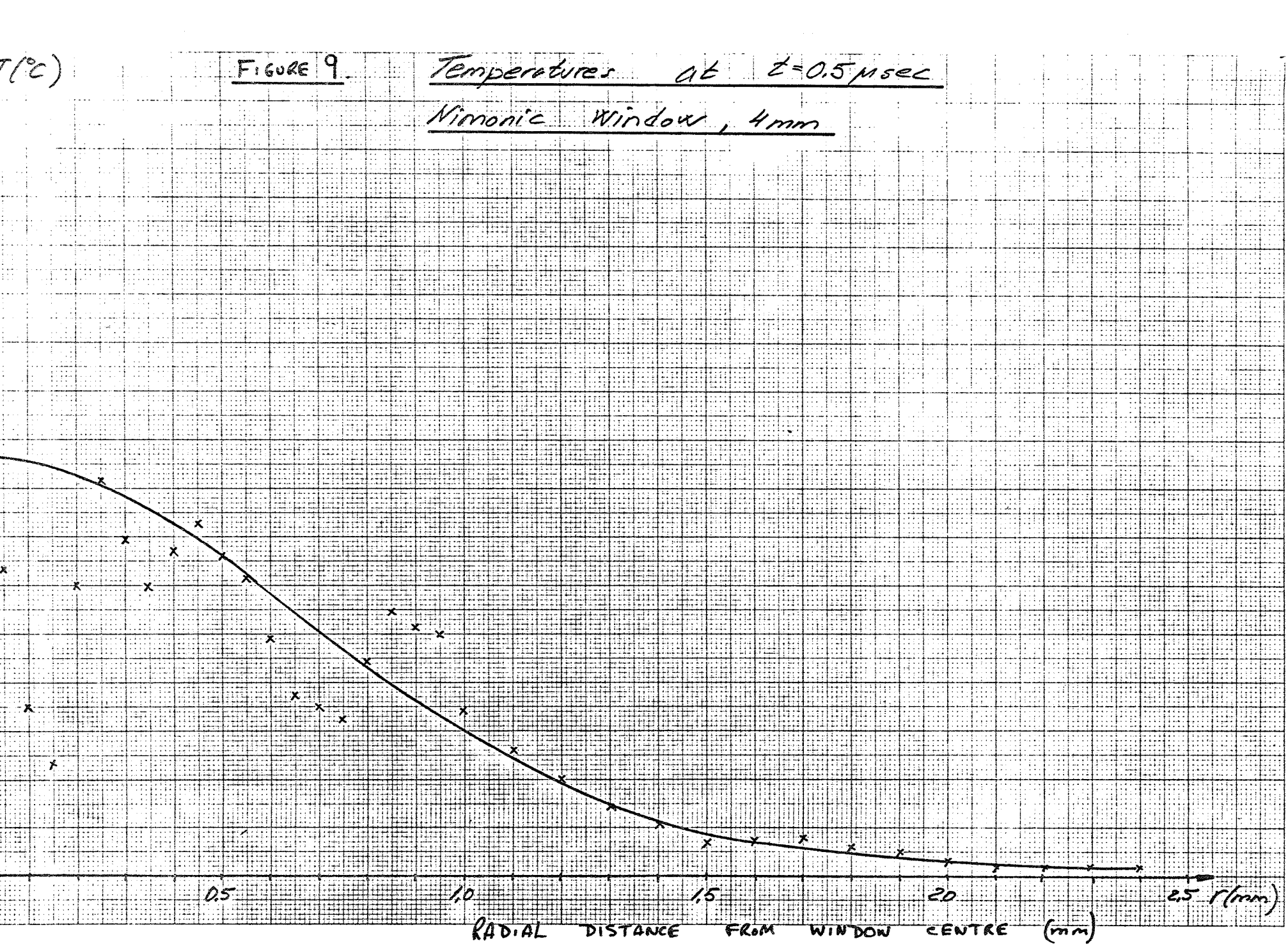

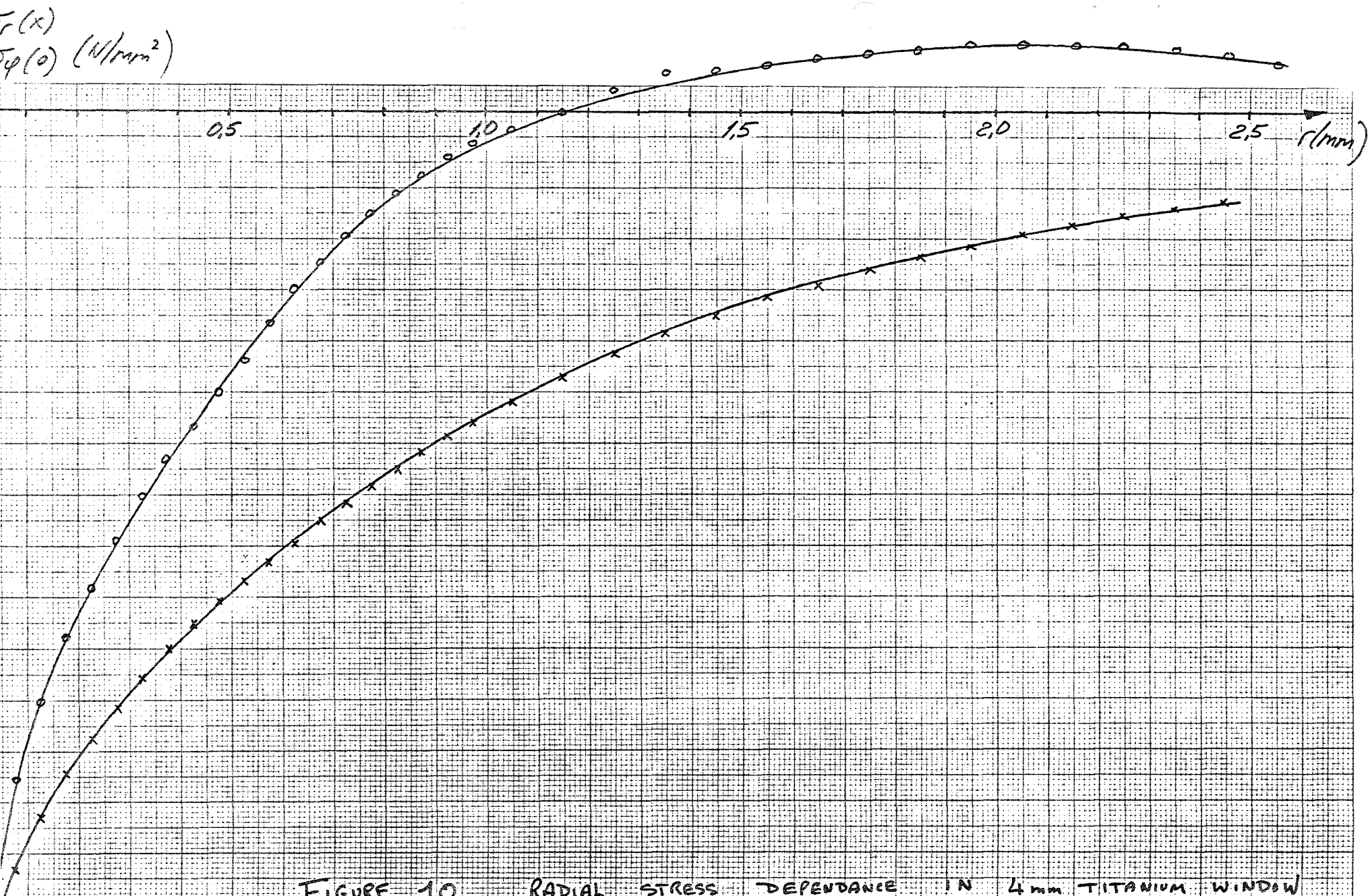

FIGURE 10. RADIAL STRESS DEPENDANCE IN 4 mm TITANIUM WINDOW

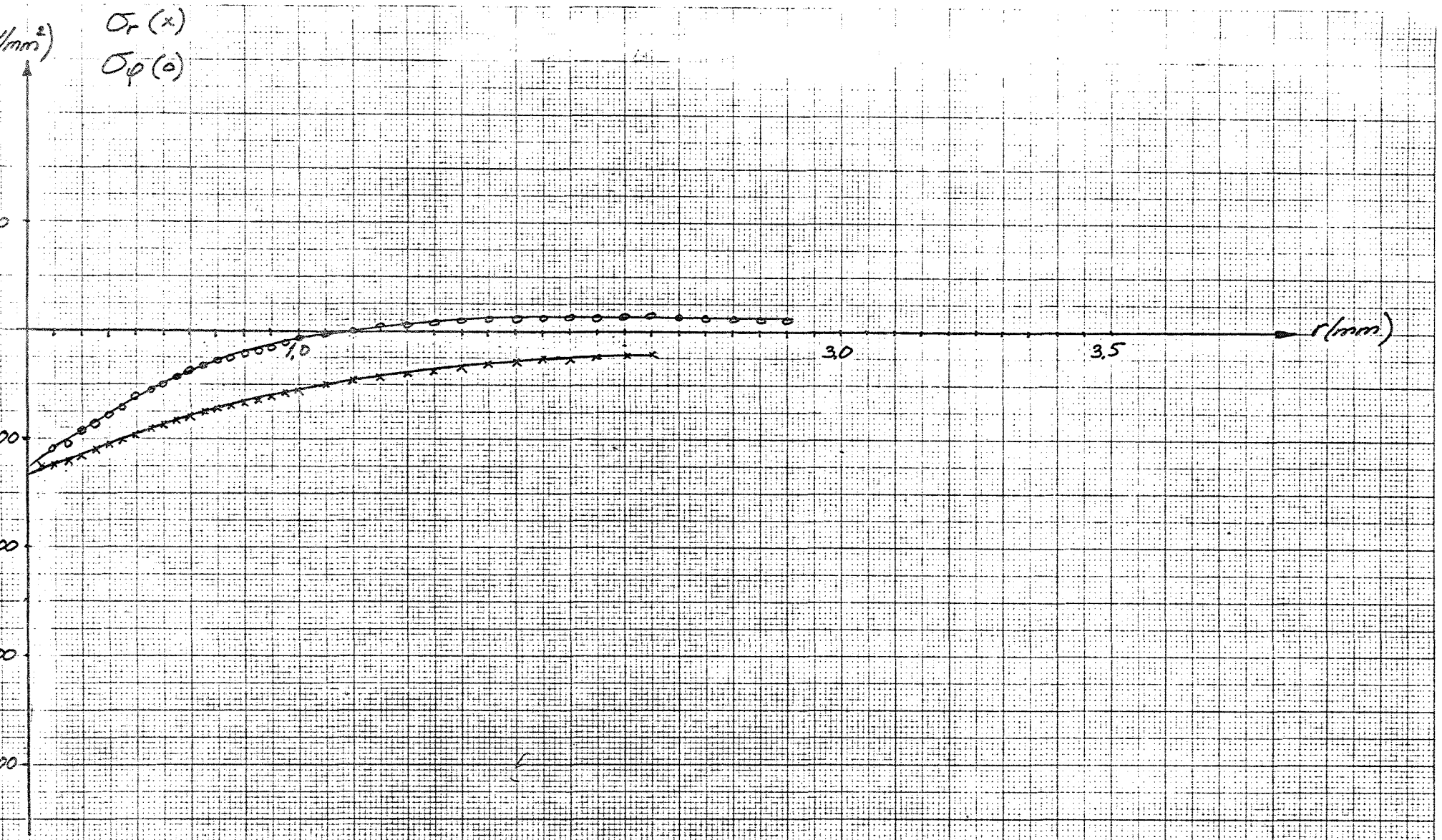

FIGURE 11. RADIAL STRESS DISTRIBUTION IN 4mm AC37 WINDOW

FIGURE 12. RADIAL STRESS DISTRIBUTIONS IN 4mm NIMONIC 105 WINDOW.

FIGURE 13C. RATIO $\frac{\sigma_{THERMAL}}{\sigma_{0,2}^{(T)}}$ AS A FUNCTION OF STEADY STATE TEMPERATURE OF WINDOW. CONVENTIONAL 12 cm COPPER TARGET.

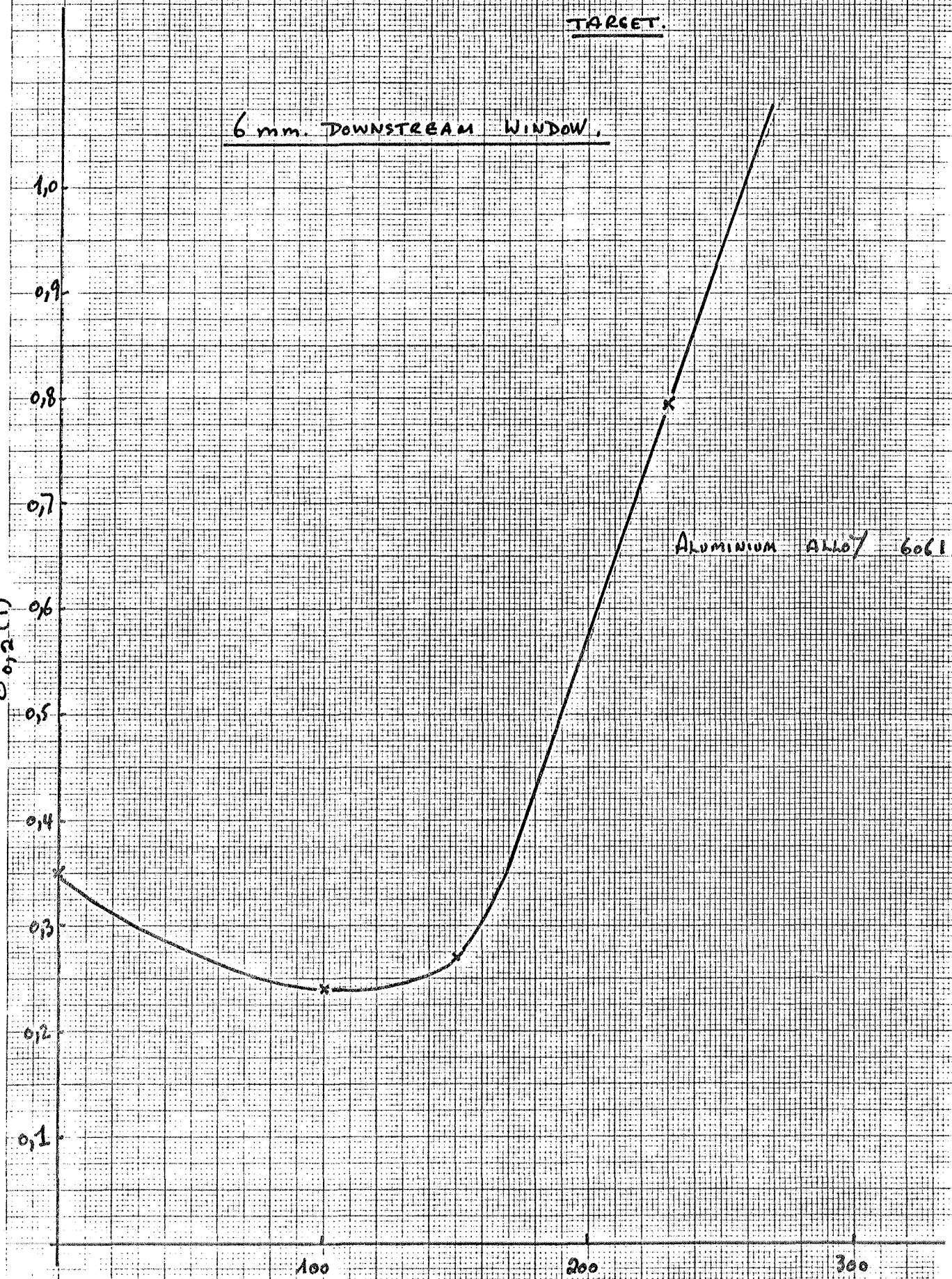

FIGURE 14. DEPOSITED ENERGY AS A FUNKTION OF RADIAL DISTANCE FROM TITANIUM WINDOW CENTRE

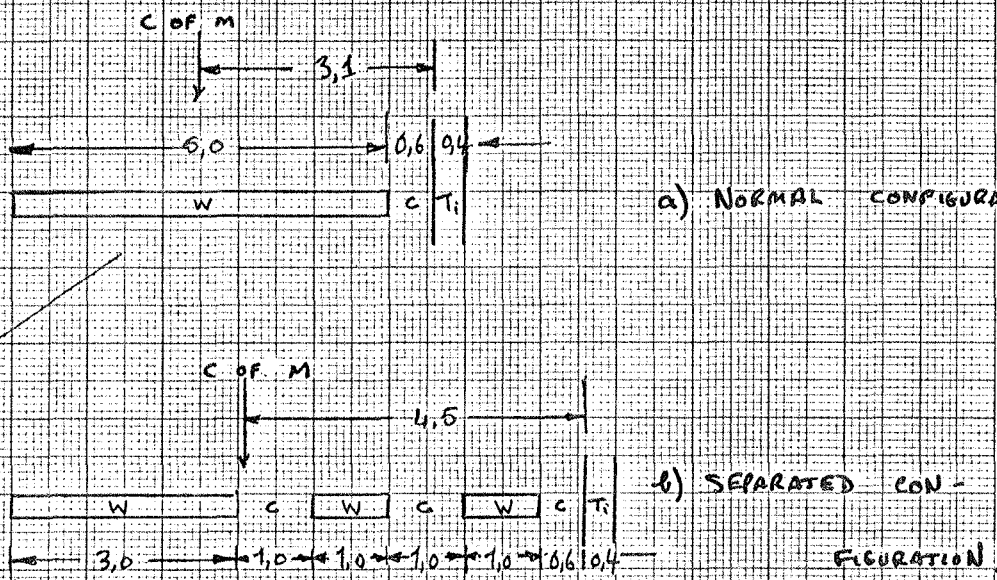

ENERGY DEPOSITED ($MeV\ cm^{-3}$)

1,0
0,9
0,8
0,7
0,6
0,5
0,4
0,3
0,2
0,1

SURE 15 ENERGY DEPOSITION IN CONVENTIONAL TUNGSTEN TARGET AS A FUNCTION OF DISTANCE ALONG TARGET, AVERAGED OUT TO $\tau = 0,15$ ms.

FIGURE 16. ENERGY DEPOSITION IN SEPARATED CONFIGURATION TUNSTEN TARGET: AS A FUNCTION OF DISTANCE ALONG TARGET, AVERAGED OUT TO $r = 0.15$ CMS

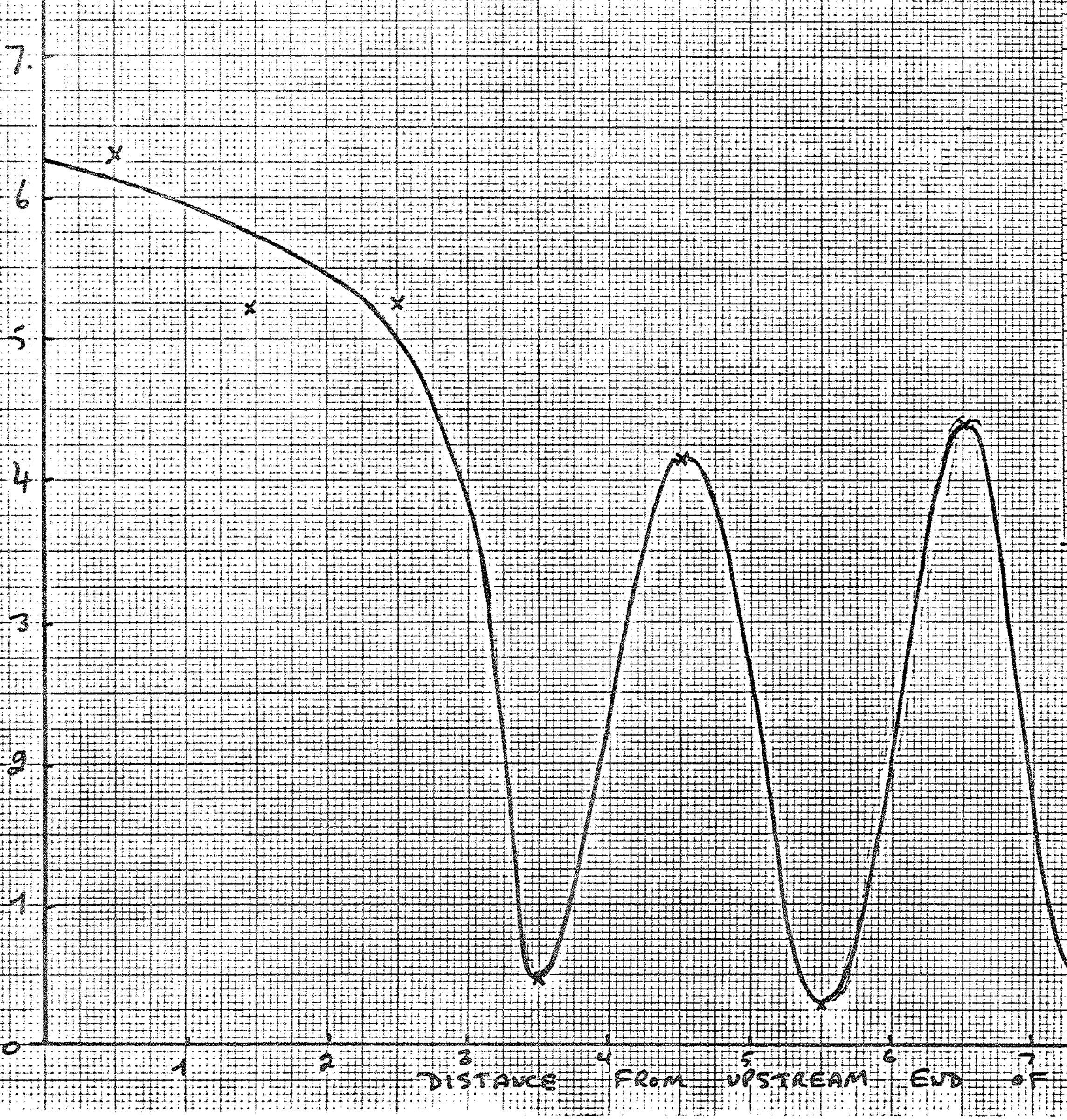

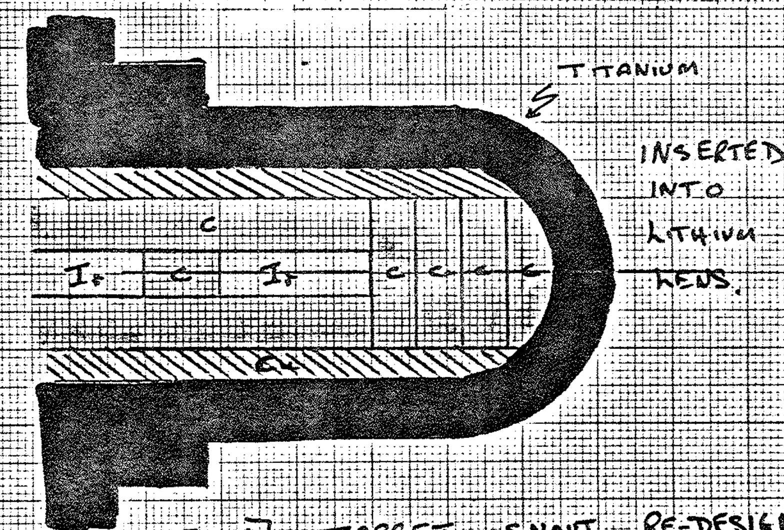

FIG 17. TARGET SNOUT RE-DESIGN

Heat-treatment 4 h/1150°C/AC + 4 h/1080°C/AC + 8 h/850°C/AC			
Test temperature °C	*Stress form*	*Stress for lives of*	
		50 h (3×10^7 cycles)	*500 h (3×10^8 cycles)*
		N/mm²	*N/mm²*
20	O ± P	348	248
	P ± 2P	155	116
	P ± P	271	209
	P ± ½P	433	356
	P ± ¼P	618	556
400	O ± P	232	232
	P ± P	193	193
	P ± ½P	371	371
	P ± ¼P	618	618
	P ± O	1004	1004
650	O ± P	271	271
	P ± P	240	240
	P ± ½P	417	417
	P ± ¼P	711	688
	P ± O	834	688
750	O ± P	263	248
	P ± P	232	209
	P ± ½P	417	371
	P ± ¼P	502	386
	P ± O	502	386
870	O ± P	240	193
	P ± P	201	155
	P ± ½P	240	155
	P ± ¼P	240	155
	P ± O	240	155
980	O ± P	170	124
	P ± P	84	46
	P ± ½P	84	46
	P ± ¼P	84	46
	P ± O	84	46

TABLE 1 FATIGUE CHARACTERISTICS OF NIMONIC 105 UNDER UNIAXIAL STRESS CYCLING.

TABLE 2. . TEMPERATURE DEPENDANT PARAMETERS OF TARGET WINDOW.

WINDOW MATERIAL : KAVORITE.

T_{melt} = 1850°C

RATURE °C.	20°	100	200	300	400	500	600	700	800
TY cm^{-3}	5.60	5,58	5,55	5.52	5,50	5,48	5,46	5.43	5,40
FIC m^{-1} °C	0,50	0,55	0,60	0,65	0,70	0,75	0,80	0,85	0,90
MAL CTIVITY m^{-1} °C	40	45	50	55	60	65	70	75	80
AR VSION ICIENT $^{-1}$ $\times 10^{-6}$	7,0	7.3	7.5	7.7	8,0	8.2	8,5	8,7	9,0
JG S ILUS mm^{-2}	120,000	118.000	115,000	111,000	106,000	101,000	94,000	88.000	80,000
LD ESS mm^{-2}	800	790	780	771	762	750	730	630	500